Supporting Information

(111) Facets-Oriented Au Decorated Carbon Nitride Nanoplatelets for Visible-Light-Driven Overall Water Splitting

Jiaxin Bai, Baichuan Lu, Qing Han, Quansong Li*, Liangti Qu**

Key Laboratory of Photoelectronic/Electrophotonic Conversion Materials, Key Laboratory of Cluster Science, Ministry of Education of China, School of Chemistry and Chemical Engineering, Beijing Institute of Technology, Beijing 100081, P. R. China. E-mail: qhan@bit.edu.cn, liquansong@bit.edu.cn, lqu@bit.edu.cn

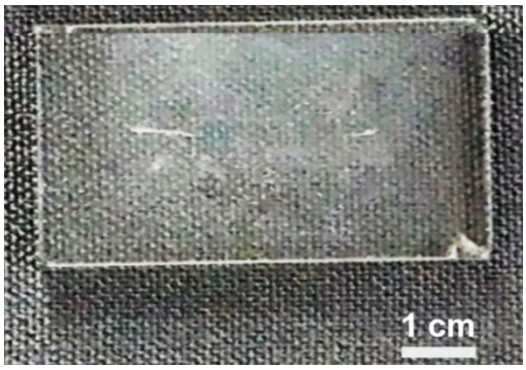

Figure S1. Photograph of the yellowish and transparent CN thin film on a quartz plate.

Table S1. The relative percentages (at%) from energy dispersive X-ray spectrum (EDS).

Element	CN	CN @Au-30	CN @Au(111)-60	CN @Au-300	CN @Au-900	CN @Au-1200
CK	37.45	51.58	49.32	54.17	55.45	39.73
NK	58.21	41.25	38.77	30.64	27.02	14.22
OK	4.34	7.09	11.20	14.14	16.32	44.59
AuM	0	0.08	0.71	1.05	1.21	1.46

It is worth noting that despite $HAuCl_4$ has been used as precursor of Au, no peak corresponding to residual Cl was observed in the EDS. This phenomenon attributed to the reheating process that leads to the reduction of Au^{3+} *in situ*.

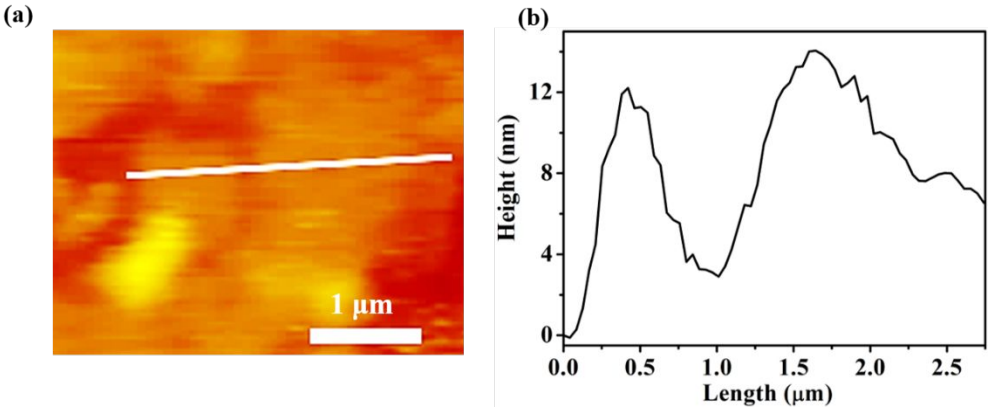

Figure S2. (a) AFM image of CN@Au(111)-60. (b) Height profile along the line in (a).

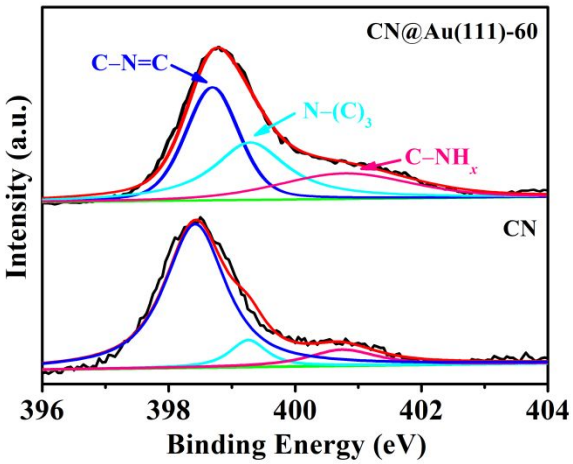

Figure S3. High-resolution N1s XPS spectra of CN@Au(111)-60 and pure CN.

Table S2. The relative percentages (at%) of the nitrogen species for and obtained from XPS.

	C–N=C	N–$(C)_3$	C–NH_x	C–N=C / (N–$(C)_3$+ C–NH_x)
CN@Au(111)-60	34.4	33.7	31.9	0.52
CN	37.4	31.2	31.4	0.60

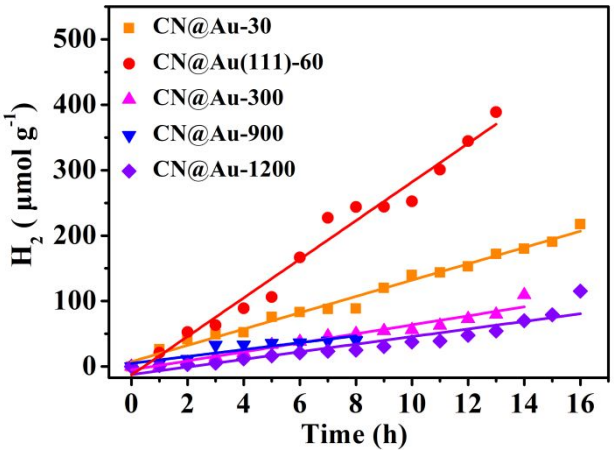

Figure S4. Hydrogen-evolution rate of CN@Au-30, CN@Au(111)-60, CN@Au-300, CN@Au-900, CN@Au-1200.

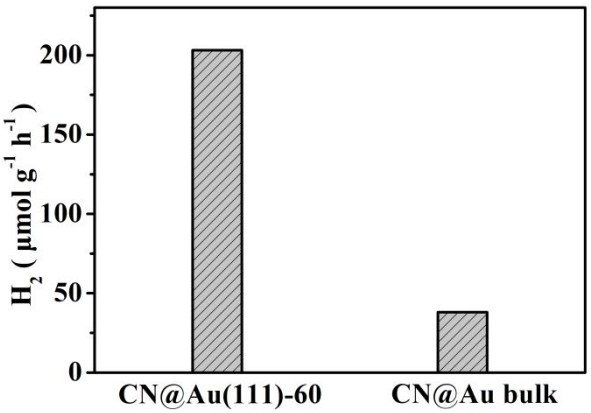

Figure S5. Hydrogen-evolution rate of CN@Au(111)-60 and CN@Au bulk.

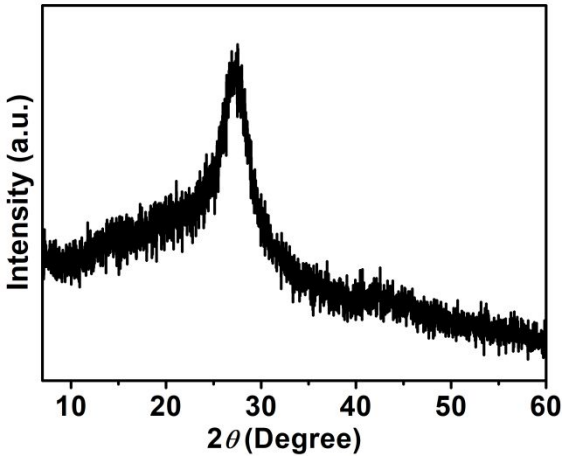

Figure S6. XRD pattern of CN@Au bulk.

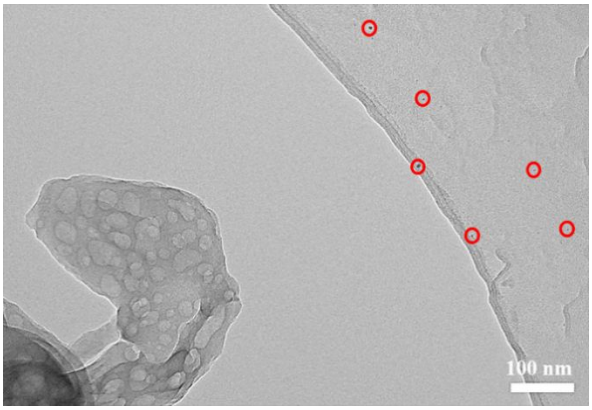

Figure S7.TEM of CN@Au bulk. (AuNPs are marked in red circles)

The sample of CN@Au(111)-60 for TEM was prepared by detaching the film from quartz substrate through ultrasonic, and the AuNPs still strongly anchored on the CN film (**Figure 2b**). However, AuNPs escaped from CN for the CN@Au bulk sample due to weak interaction between AuNPs and CN.

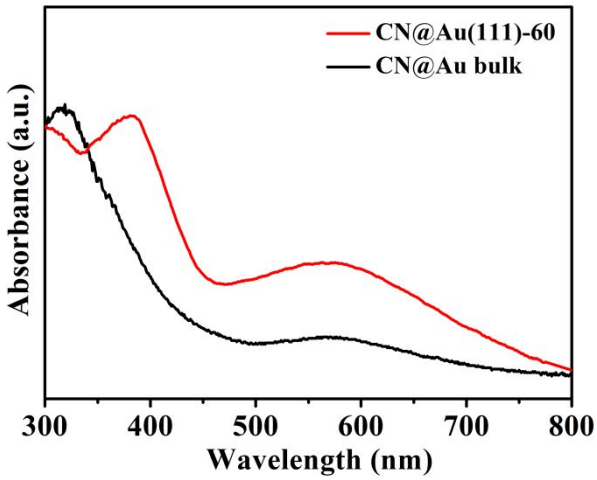

Figure S8. UV-Vis absorption curves of CN@Au(111)-60 and CN@Au bulk.

Comparing with CN@Au(111)-60, there is no obvious bathochromic-shift in the spectrum of CN@Au bulk, which is bad for visible light absorption during photocatalytic process.

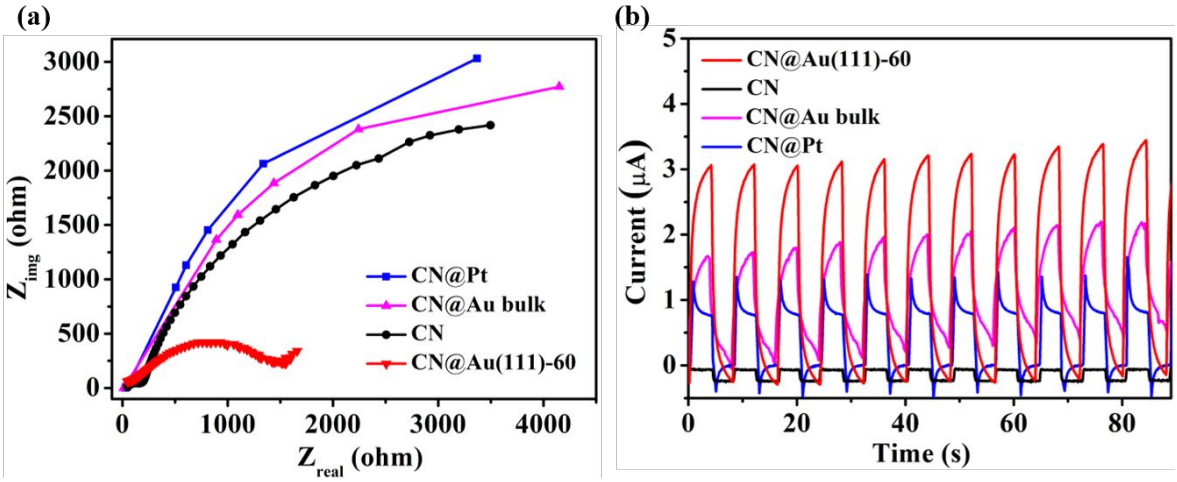

Figure S9. (a) EIS Nyquist plots and (b) Transient photocurrents responses of CN@Au(111)-60, CN, CN@Au bulk and CN@Pt.

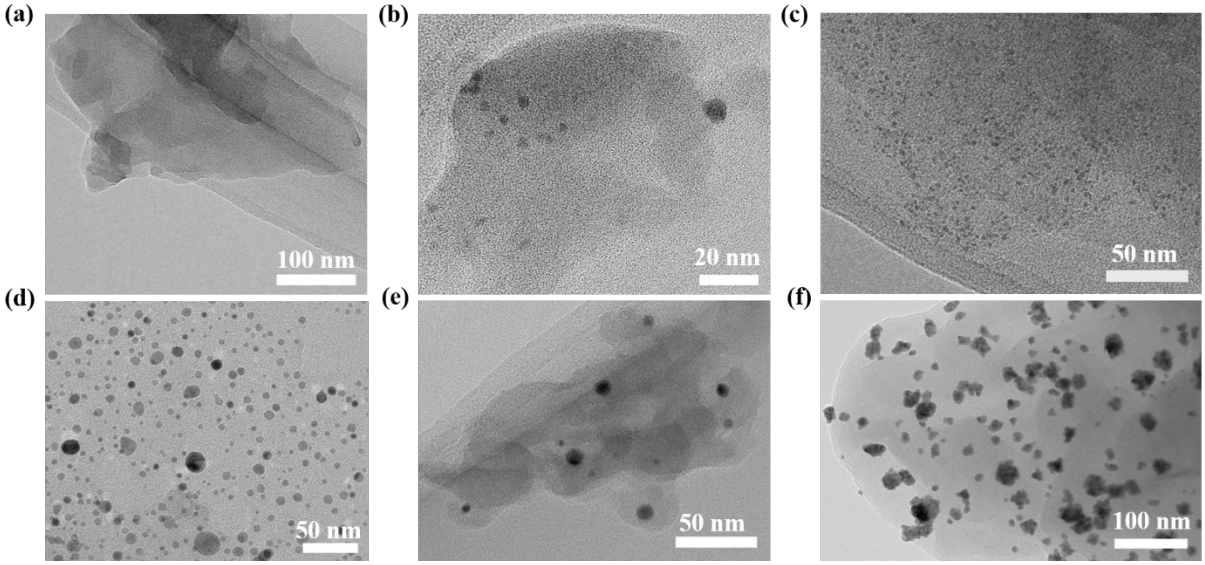

Figure S10. TEM images of (a) CN, (b) CN@Au-30, (c) CN@Au(111)-60, (d) CN@Au-300, (e) CN@Au-900, (f) CN@Au-1200, respectively.

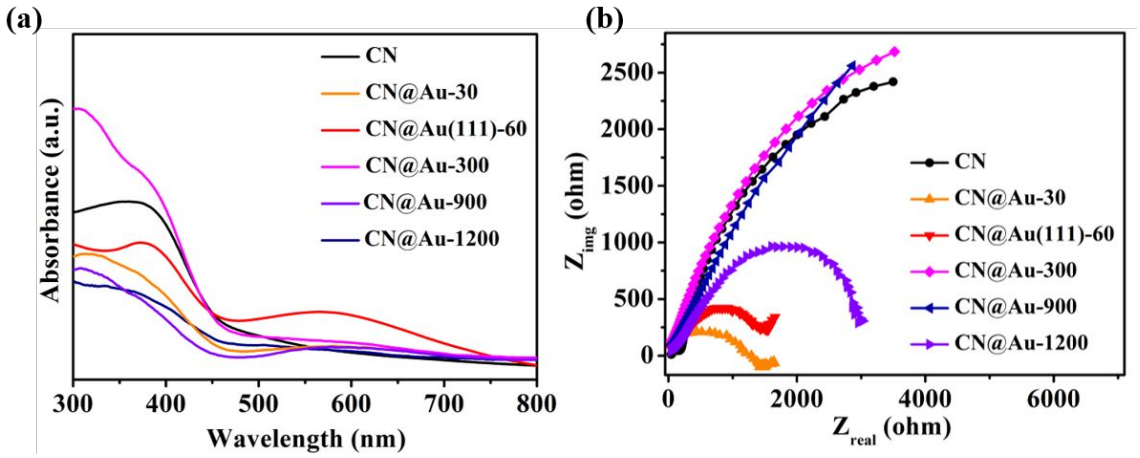

Figure S11. (a) UV-Vis absorption curves and (b) EIS Nyquist plots of CN, CN@Au-30, CN@Au(111)-60, CN@Au-300, CN@Au-900 and CN@Au-1200, respectively.

A further increase of impregnating time causes decreased light harvesting and large internal resistances, which are adverse to photocatalytic activity.

Table S3. The relative percentages (at%) from energy dispersive X-ray spectrum (EDS).

Element	CN@Pt
CK	44.16
NK	54.19
OK	1.51
PtM	0.14

As shown in Table S3, no peak corresponding to the residual Cl can be measured in the EDS after UV-light ridiation, verifing the Pt^{2+} from H_2PtCl_4 precursor was reduced.

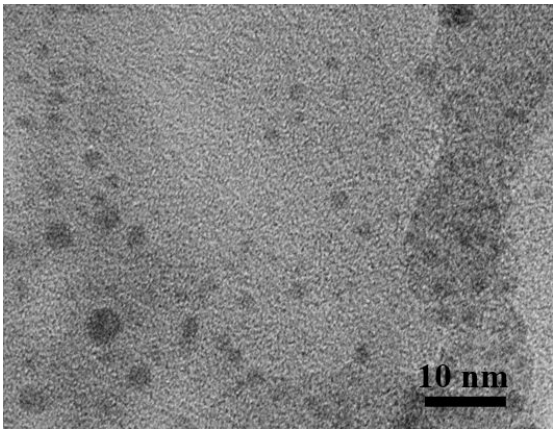

Figure S12. TEM image of CN@Au(111)-60 after a 12-h stability measurement.

The black dots in this image represent Au nanoparticles strong grafting on the CN nanosheets after the photocatalytic reaction.

Table S4. The relative percentages (at%) of CN@Au(111)-60 after a 12-h stability measurement from energy dispersive X-ray spectrum (EDS).

Element	CN@Au(111)-60
CK	50.61
NK	31.46
OK	17.43
AuM	0.50

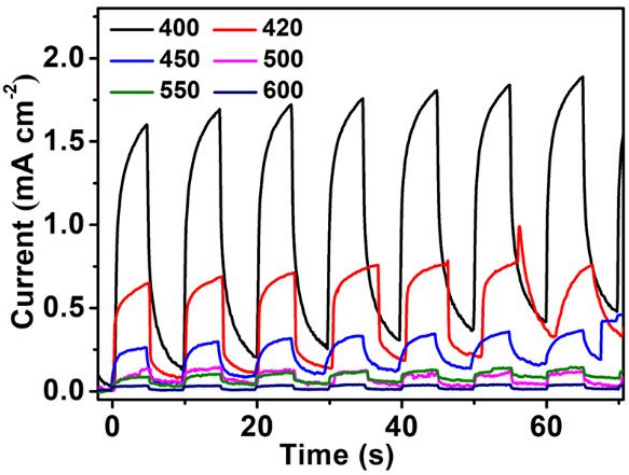

Figure S13. Wavelength dependence of transient photocurrents (λ =400, 420, 450, 500, 550, 600 nm) of CN@Au(111)-60.